Vietnam Journal of Mechanics, Vol. 46, No. 2 (2024), pp. 93 – 103
DOI: https://doi.org/10.15625/0866-7136/20106

APPLICATION OF NEWLY PROPOSED HARDENING LAWS FOR STRUCTURAL STEEL RODS

Van Nam Nguyen[1], **Duy Triet Doan**[2], **Nhat-Phi Doan**[1,*]
[1]*Department of Civil Engineering, Industrial University of Ho Chi Minh City, Vietnam*
[2]*Department of Mechanical Dynamics, Vinh Long University of Technology Education, Vinh Long, Vietnam*
[*]E-mail: doannhatphi@iuh.edu.vn

Received: 07 February 2024 / Revised: 10 April 2024 / Accepted: 23 April 2024
Published online: 04 June 2024

Abstract. In civil engineering, distinct mechanical properties and behaviors of structural steel rods necessitate a novel approach to material modeling. This study extends the application of recently proposed strain-hardening laws, originally developed for automotive sheet metals, to several structural steel rods (CB240-T and CB300-T). Standard uniaxial tensile tests are conducted for each examined material to obtain experimental stress-strain data. Various curve fitting methods are then employed to refine the parameters of the strain-hardening laws, enabling accurate representation of the steel rods mechanical behavior. Subsequently, these laws are implemented in Abaqus software for numerical simulation of uniaxial tensile tests, facilitating the analyses of material response under uniaxial tensile loading condition. Compared to the measured data, the predicted force-displacement curves are in good agreement with the measurements until the tail of the curves. The comparisons verify the ability and potential of the examined hardening law for studying the post-necking behavior of structural steels. The outcomes provide a framework for more precise characterization of structural steel materials.

Keywords: structure steel rods, hardening law, post-necking, finite element analysis, uniaxial tensile test.

1. INTRODUCTION

Structural steel rods are widely used in building constructions and civil engineering due to their high strength and toughness. Plastic deformations induce the so-called hardening behavior of steel rods that significantly affects material properties [1, 2]. Understanding this mechanical behavior plays a crucial role for ensuring the safety and

reliability of structures. Therefore, accurate modeling of the hardening behavior of steel rods is mandated to evaluate the collapse resistant capacity of structures. Traditionally, material models for structural steel have relied on simple linear elastic or isotropic hardening laws to simulate their behavior under stress. However, these models often fail to capture the nonlinear and post-necking behaviors exhibited by steel rods, particularly under extreme loading conditions [3,4].

Descriptions of strain hardening behavior of steel materials have been investigated for many years. The hardening responses are commonly characterized by true stress-strain curves obtained from uniaxial tensile tests. Furthermore, the captured hardening behavior is then reproduced mathematically by a hardening law. Many formulas have been proposed to describe the hardening behavior of different steel materials, for example, Ramberg and Osgood [5], Hollomon [6], Swift [7], Ludwigson [8]. Within each formula, application of the hardening law for a wide variety of materials is a challenge, although excellent results have been provided for specific materials. These formulas have been extended in different ways to broaden their application in practical use [9–11]. These extended formulas require more parameters to reproduce the hardening behavior of the investigated materials. The act always increases the number of parameters involved to the hardening law formulation, that raises difficulty in calibrating these parameters.

Recently, several formulas have been proposed by one of the authors to provide a better description of the hardening behavior of automotive sheet metals [12, 13]. Benefits of these proposed formulas, such as high flexibility within a requirement of four parameters were demonstrated in previous studies for automotive aluminum alloy and steel sheets [14,15]. It is worth noticing that the chemical components of structural steels differ significantly from those of automotive materials. In detail, the percentage of carbon in the former is extremely higher than those of the latter. The difference leads to phase-transform phenomenon which are frequently observed structural steels. Due to the occurrence of phase transformations, the stress-strain curves of structural steels are conventionally divided into different stages of deformation [16]. That makes describing the hardening behavior of structural steels by a single function more difficult, in comparing to automotive steels.

This study examines the potential of newly proposed hardening laws for several structural steel rods including CB240-T and CB340-T materials. The rest of the paper is structured as follows. Section 2 presents in detail the uniaxial tensile tests that were conducted to achieve the experimental hardening behaviors of the tested materials. Formulations of the examined hardening laws are revisited in Section 3. Parameters of these hardening laws are then identified by a common curve fitting method. Section 4 validates the usefulness of the identified hardening laws in simulating the uniaxial tensile tests for

all investigated materials. Section 5 summarizes and discusses the work's perspectives and limitations.

2. EXPERIMENT

The tested materials in this study are structural steel rods CB240-T and CB300-T with diameters of 6 mm and 8 mm, respectively. These materials are widely used in civil engineering and construction. Uniaxial tensile tests are conducted following the Vietnamese standard TCVN 1651-1:2018 [17]. During experimental tests, a specimen which is prepared with an initial length of 250 mm is pulled with a constant crosshead speed of 3 mm/min until failure. The loads acting on the specimen are recorded by a load-cell, while the displacement of an initial gauge length is recorded. Fig. 1 shows force-displacement curves obtained from three tests conducted for each investigated material to verify the repeatability. For both materials, the derived force-displacement curves and maximum forces are in high agreements until the tail of the curves, where presents a moderate difference in the data of Test 2 data (for CB240-T) and Test 3 data (for CB300-T) comparing to other test samples. Thus, the curve obtained from the first test of each examined material is used to calculate the stress-strain curves, which are reported in Fig. 2. It is seen that the yield points are approximately 8.3 MPa at 2.5 mm of displacement for CB240-T and 13.2 MPa at 2.8 mm of displacement for CB300-T, respectively. Prior to this point is the elastic region. Following this point is the hardening phase until the CB240-T experiences maximum stresses of around 11.7 MPa at approximately 42.7 mm displacement, and 21.7 MPa at 47.8 mm displacement for CB300-T, in line with the maximum forces. Beyond this threshold, the mechanical behavior transitions into the post-necking

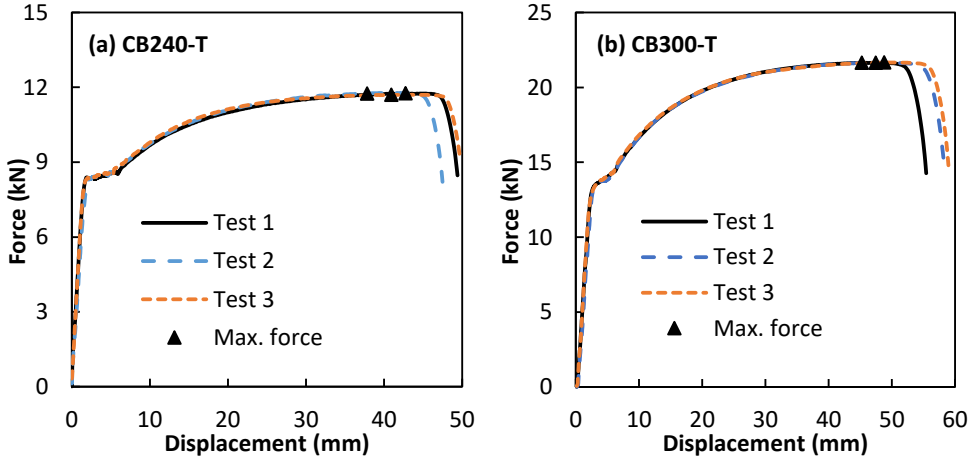

Fig. 1. Force-displacement curves obtained from three uniaxial tensile tests for two tested materials (a) CB240-T and (b) CB300-T

region, which enables the rapid decrease of stress over a short relative displacement until the fractures occur.

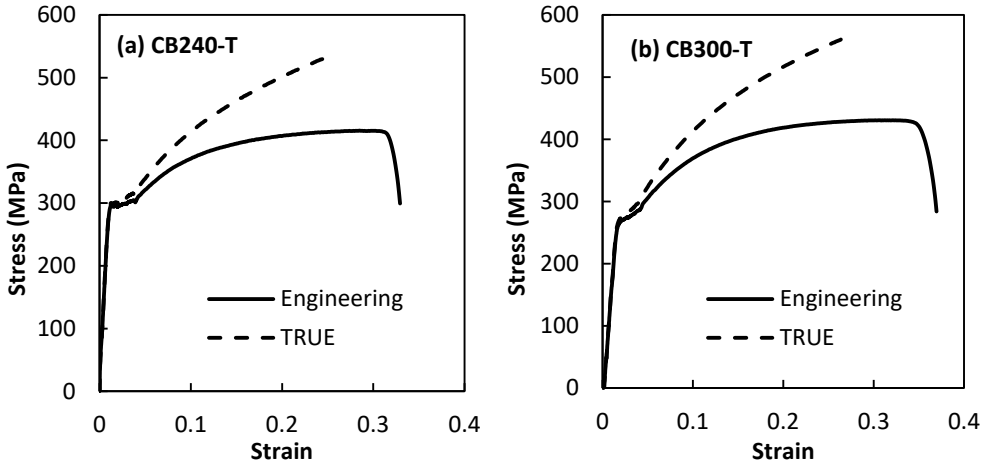

Fig. 2. Stress-strain curves of the tested materials obtained from the uniaxial tensile test (a) CB240-T and (b) CB300-T

The stress-strain curve for a material is constructed by elongating the sample and recording the stress variation with strain until the sample fractures. It is often presumed that the cross-sectional area of the material remains constant throughout the entire deformation process. However, this assumption is inaccurate as the actual area decreases during deformation due to both elastic and plastic deformation. The curve originating from the initial cross-sectional area and gauge length is termed the 'engineering' stress-strain curve, also known as nominal stress-strain curve (i.e., continuous line in Fig. 2), while the curve originating from the instantaneous cross-sectional area and length is termed the 'true' stress-strain curve (i.e., dash line in Fig. 2). The detailed procedure to determine engineering stress-strain curves and true stress-strain curves can be found in the Abaqus software manual [18]. An obvious observation is that the true stress-strain curve consistently maintains or increases its value. This is attributed to the fact that the material does not weaken. The decrease in the engineering stress is an illusion created because the engineering stress does not consider the decreasing cross-sectional area of the sample.

3. CONSTITUTIVE MODEL

3.1. Hardening models

The most widely used hardening constitutive for steel materials is the model proposed by Swift [5] of which the formulation is expressed as

$$\text{Swift:} \qquad \sigma = c_1 \left(c_2 + \bar{\varepsilon}\right)^{c_3}, \tag{1}$$

where σ is the flow stress, $\bar{\varepsilon}$ is the equivalent plastic strain, and $c_1 \sim c_3$ are material parameters that are needed to be identified. Although this model has been widely used for many steel materials, it seems to be lack of the flexibility to reproduce the entire stress-strain relationship for many sheet metals, especially in the post-necking regimes [19–22]. Recently, Pham and Kim [12] proposed a multiplicative hardening law (labelled by "Model 2") for sheet metals expressed as the follows

$$\text{Model 2:} \qquad \sigma = c_1 + c_2 \left(1 - \exp\left(-c_2\bar{\varepsilon}\right)\right)\left(0.002 + \bar{\varepsilon}\right)^{c_4}. \tag{2}$$

Furthermore, improvements of the Swift hardening law were proposed [11]. Based on these models (labelled by "Model 3" and "Model 4"), the flow stress can be calculated as the follows

$$\text{Model 3:} \qquad \sigma = c_1 \left(2 - \exp\left(-c_2\bar{\varepsilon}\right) + c_3\bar{\varepsilon}\right)^{c_4}, \tag{3}$$

$$\text{Model 4:} \qquad \sigma = c_1 \left(1 + \frac{c_2\bar{\varepsilon}}{\left[1 + \left(c_3\bar{\varepsilon}\right)^4\right]^{1/c_4}}\right). \tag{4}$$

These proposed hardening laws contain four parameters. Their capacity in capturing the hardening behavior of several automotive sheet metals has been proved in the previous study [11].

3.2. Parameter identification

The most widely used method for parameter identification is numerical fitting. The method is available in calculation packages such as Excel, Matlab, etc. In this calibration method, a cost function is constructed based on the difference between the experimental data and the hardening law's predictions as follows

$$f = \sum_{i=1}^{N} \left(\sigma_i^{exp} - \sigma_i^{pre}\right)^2, \tag{5}$$

where σ_i^{exp} and σ_i^{pre} denote the experimental and predicted stresses, N denotes the number of total data. An optimization algorithm, such as general gradient decent, is applied to determine parameters by minimizing the cost function. The goodness of the identified hardening law is estimated by the coefficient of determination, of which formulation is expressed as follows

$$R^2 = 1 - \frac{\sum \left(\sigma_i^{exp} - \sigma_i^{pre}\right)^2}{\sum \left(\sigma_i^{exp} - \mu_\sigma\right)^2}, \tag{6}$$

where μ_σ is the mean value of all experimental stresses. The aforementioned fitting method is applied to identify parameters of all considering hardening laws for two tested materials.

3.3. Comparison

Table 1 reports parameters of the identified hardening laws for both two materials along with the cost function and R^2 coefficient. In addition, Fig. 3(a) and Fig. 4(a) illustrate the flow curves of these materials predicted by the examined hardening laws in comparison to the experimental data. Moreover, Fig. 3(b) and Fig. 4(b) depict the extrapolation of these hardening laws to an extensive strain range.

Table 1. Identification of hardening law's parameters and their evaluation

	Model	c_1	c_2	c_3	c_4	f	R^2
CB240-T	Swift	781.13 MPa	0.0315	0.2651	-	84.9 MPa^2	0.99993
	Model 2	316.16 MPa	589.12	61.65	0.630	387.9 MPa^2	0.99967
	Model 3	312.73 MPa	9.03	15.18	0.333	84.0 MPa^2	0.99993
	Model 4	311.98 MPa	9.75	3.74	0.594	101.4 MPa^2	0.99991
CB300-T	Swift	840.11 MPa	0.0278	0.290	-	232.2 MPa^2	0.99982
	Model 2	305.71 MPa	631.92	45.38	0.602	618.4 MPa^2	0.99953
	Model 3	300.0 MPa	10.32	4.18	0.601	31.3 MPa^2	0.99998
	Model 4	299.26 MPa	9.63	4.37	0.760	33.3 MPa^2	0.99998

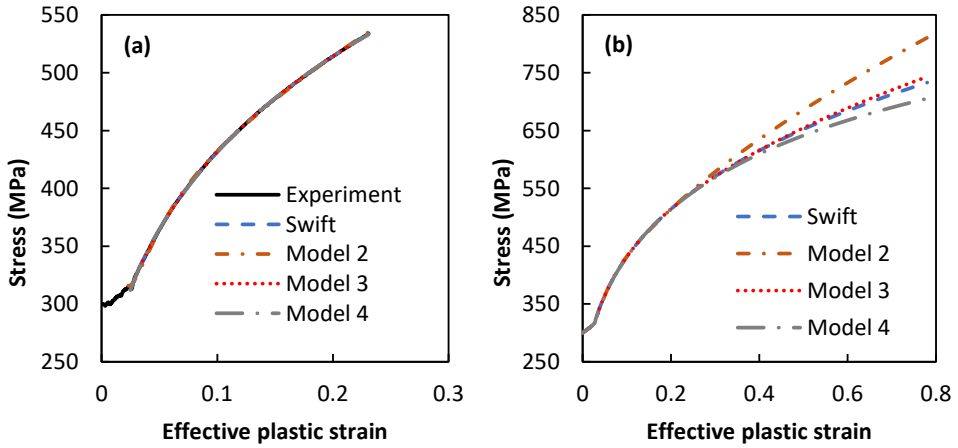

Fig. 3. Identified hardening laws compared to the experimental data of CB240-T material (a) Fitting results and (b) Extrapolation to a large strain range

According to Table 1, all considering hardening laws give good approximations for the experimental data where the coefficient of determination, R^2 is always higher than

0.999. In the case of CB240-T materials, the highest cost function of 387.9 MPa^2 and the lowest R^2 are observed by Swift model. Whereas the highest cost function of 618.4 MPa^2 and the lowest R^2 for CB300-T material is observed in the case of Model 2. Furthermore, Model 3 and Model 4 yield extremely good cost functions and coefficient of determination for both two materials, especially compared to those of the others. The comparison indicates the flexibility of these two hardening models for reproducing the hardening behaviors of steel materials.

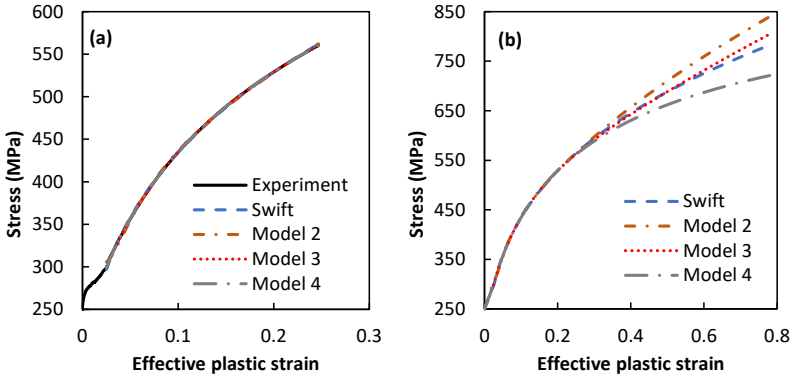

Fig. 4. Identified hardening laws compared to the experimental data of CB300-T material (a) Fitting results (b) Extrapolation to a large strain range

As seen in Fig. 3(a) and Fig. 4(a), all of these hardening laws present excellent approximations for the experimental data up to around 0.25 of effective plastic strain, for both CB240-T and CB300-T materials. However, their extrapolations to large strain ranges (i.e., beyond 0.3 of effective plastic strain) show significant deviations as shown in Fig. 3(b) and Fig. 4(b). The stresses at the transition points are predicted at around 569 MPa for CB240-T and 589 MPa for CB300-T, respectively. Model 2 always gives the highest predictions in large strain ranges; Model 4 gives the lowest predictions. The forecasts of Model 3 and Swift are close together. A slight deviation is observed where the prediction of Model 3 is foremost linear in the extensive strain ranges, while, those of Swift shows a nonlinear curvature. The observation is explainable from the formulation of Model 3 where the contribution of the linear term (i.e. $c_3\bar{\varepsilon}$) exceeds those of the non-linear term (i.e. $\exp(-c_2\bar{\varepsilon})$) in the large strain ranges.

4. FINITE ELEMENT ANALYSIS

A finite element model is developed in Abaqus/Explicit software [18] to simulate the uniaxial tensile tests for both materials. Eight-node solid elements with reduced integration (C3D8R) with a total of 5168 elements are used to model the steel rods. The steel rods

have a length of 250 mm with a diameter of 6mm for CB240-T and 8 mm for CB300-T, respectively. Fig. 5 shows mesh generation on the FE specimen. The maximum mesh size is not exceeded 2 mm. During simulations, one end of the rod is fixed and a constant velocity, replicating to the constant crosshead speed of 3 mm/min in experiments, is applied to the another end. Mises yield function [18] is coupled with the identified hardening laws (obtained from Section 3) to describe the plastic deformation of the tested materials.

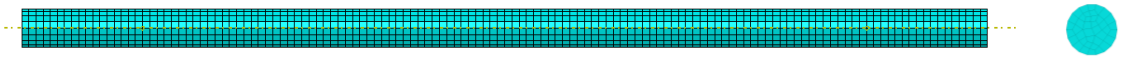

Fig. 5. Mesh generation in these simulations of CB300-T specimen

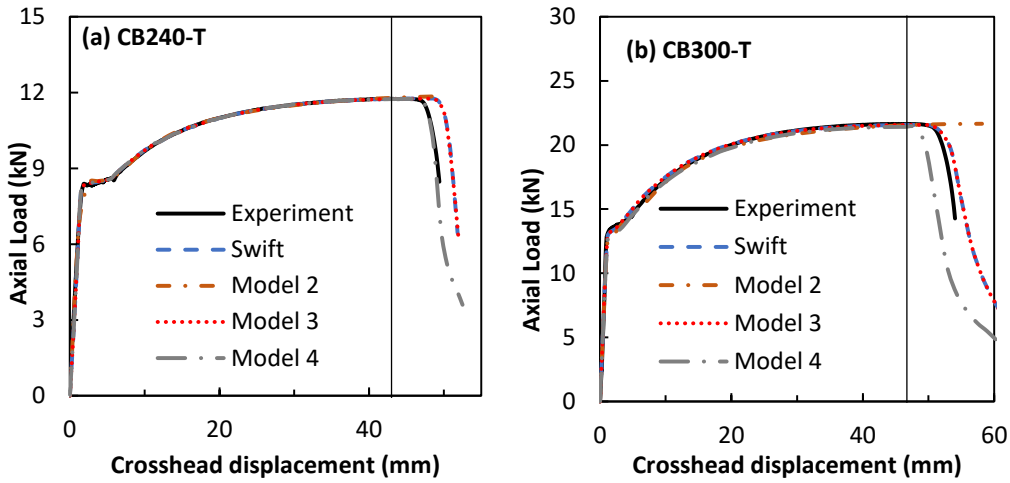

Fig. 6. Comparison between the predicted forces based on the examined hardening laws and the measured data (a) CB240-T and (b) CB300-T

After simulations, the predicted axial forces based on these hardening laws are compared to the experimental data and reported in Fig. 6. The vertical line in this figure indicates the measured crosshead displacement of the maximum loading force measured in the experiments (i.e., 11.7 MPa at 42.7 mm displacement for CB240-T, and 21.7 MPa at 47.8 mm displacement for CB300-T). As seen in Fig. 6, all of these hardening laws yield good predictions for axial loads up to the maximum force. It can be said that all hardening laws adopted in this study are perfect applicable to the hardening behavior the structural steel rods. Slight differences are observed at the tails of these curves (i.e., post-necking behavior), where the predictions of Model 2 overestimate the experimental data of the two materials. Swift and Model 3 give similar predictions during the entire loading forces process, which are more or less comparable to the measured data of CB240-T and CB-300-T, respectively. Model 4 provides excellent prediction for the experimental

curves of the tested materials, especially for CB240-T rod. Comparisons clarify the potential application of Model 3 and Model 4 in reproducing the hardening behavior of structural steels.

5. CONCLUSIONS

This study examined the ability of four hardening laws in reproducing the hardening behaviors of two steel rods. These hardening laws include a well-established model proposed by Swift and three newly proposed models which were initially introduced for automotive sheet metals. It is seen that all of these models are able to capture well the experimental data obtained from uniaxial tensile tests of CB240-T and CB300-T steel rods. Comparison between simulated and measured loading forces during the testes pointed out that the applications of Model 4 for the tested materials are very promising, while predictions of Model 3 are mostly identical to those of Swift model in the current examinations. Future studies on their applications for structural steels are deserved for further investigations. However, the predictions of Model 2 seem to overestimate the experimental data of two materials. Care should be taken in applying this model for different structural steel materials, especially for predictions in the large strain ranges. Use of an advanced calibration method may improve its accuracy of post-necking prediction.

Although the promising results and insights are provided by this study, several limitations and assumptions can be drawn as following:

- The study focused on limited materials with two specific types of structural steel rods (CB240-T and CB300-T). This requires additional calibration and validation on other steel grades and structural steel plates to cover the structural steel in civil engineering;

- Uniaxial tensile tests were used to evaluate the performance of the hardening laws. While this provides valuable data, variation of loading conditions such as compression, combined loading, fatigue loading or cyclic loading on structural rods are often more complex and must be taken into account in reality;

- The Von-Mises model used in the analysis assumes the material homogeneity and the strain isotropy, which may not always be the case in practical scenarios. Heterogeneities in material properties, caused by factors such as manufacturing processes or structural defects, have the potential to affect the accuracy of the predictions;

- The mesh size being used is assumed to be sufficient to capture the deformation of the material in the large deformation zone (post-necking behavior);

- The analyses do not account for the strain rate sensitivity of structural steel rods, where the material mechanical properties can vary depending on the rate at which it is deformed.

DECLARATION OF COMPETING INTEREST

The authors declare that they have no known competing financial interests or personal relationships that could have appeared to influence the work reported in this paper.

ACKNOWLEDGMENT

The support of this research by Industrial University of Ho Chi Minh City and Vinh Long University of Technology Education is gratefully acknowledged. The authors also thank Dr. Quoc Tuan Pham - Department of Mechanical Engineering, Blekinge Institute of Technology, Karlskrona, Sweden for his support with the computer code of the new strain-hardening laws for automotive sheet metals.

REFERENCES

[1] M. B. Jabłońska, K. Kowalczyk, M. Tkocz, R. Chulist, K. Rodak, I. Bednarczyk, and A. Cichański. The effect of severe plastic deformation on the IF steel properties, evolution of structure and crystallographic texture after dual rolls equal channel extrusion deformation. *Archives of Civil and Mechanical Engineering*, **21**, (2021). https://doi.org/10.1007/s43452-021-00303-6.

[2] A. A. Shah and Y. Ribakov. Recent trends in steel fibered high-strength concrete. *Materials & Design*, **32**, (2011), pp. 4122–4151. https://doi.org/10.1016/j.matdes.2011.03.030.

[3] S. L. Chan. Non-linear behavior and design of steel structures. *Journal of Constructional Steel Research*, **57**, (2001), pp. 1217–1231. https://doi.org/10.1016/s0143-974x(01)00050-5.

[4] Z.-J. Zhang, B.-S. Chen, R. Bai, and Y.-P. Liu. Non-linear behavior and design of steel structures: Review and outlook. *Buildings*, **13**, (2023). https://doi.org/10.3390/buildings13082111.

[5] W. Ramberg and W. R. Osgood. Description of stress-strain curves by three parameters. Technical report, National Advisory Committee for Aeronautics, (1943).

[6] J. H. Hollomon. Tensile deformation. *Transactions of AIME*, **162**, (1945), pp. 268–290.

[7] H. W. Swift. Plastic instability under plane stress. *Journal of the Mechanics and Physics of Solids*, **1**, (1952), pp. 1–18. https://doi.org/10.1016/0022-5096(52)90002-1.

[8] D. C. Ludwigson. Modified stress-strain relation for FCC metals and alloys. *Metallurgical Transactions*, **2**, (1971), pp. 2825–2828. https://doi.org/10.1007/bf02813258.

[9] N. Y. Golovina. The nonlinear stress-strain curve model as a solution of the fourth order differential equation. *International Journal of Pressure Vessels and Piping*, **189**, (2021). https://doi.org/10.1016/j.ijpvp.2020.104258.

[10] A. Lavakumar, S. S. Sarangi, V. Chilla, D. Narsimhachary, and R. K. Ray. A "new" empirical equation to describe the strain hardening behavior of steels and other metallic materials. *Materials Science and Engineering: A*, **802**, (2021). https://doi.org/10.1016/j.msea.2020.140641.

[11] T. Li, J. Zheng, and Z. Chen. Description of full-range strain hardening behavior of steels. *SpringerPlus*, **5**, (2016). https://doi.org/10.1186/s40064-016-2998-3.

[12] Q. T. Pham and Y. S. Kim. Identification of the plastic deformation characteristics of AL5052-O sheet based on the non-associated flow rule. *Metals and Materials International*, **23**, (2017), pp. 254–263. https://doi.org/10.1007/s12540-017-6378-5.

[13] Q. T. Pham and Y.-S. Kim. Evaluation on flexibility of phenomenological hardening law for automotive sheet metals. *Metals*, **12**, (2022). https://doi.org/10.3390/met12040578.

[14] Q. T. Pham, H. S. Le, A. T. Nguyen, X. Xiao, Y.-S. Kim, V. D. Nguyen, H. S. Tran, and X. Van Tran. A machine learning–based methodology for identification of the plastic flow in aluminum sheets during incremental sheet forming processes. *The International Journal of Advanced Manufacturing Technology*, **120**, (2022), pp. 3559–3584. https://doi.org/10.1007/s00170-022-08698-z.

[15] Q. T. Pham, T. Nguyen-Thoi, J. Ha, and Y.-S. Kim. Hybrid fitting-numerical method for determining strain-hardening behavior of sheet metals. *Mechanics of Materials*, **161**, (2021). https://doi.org/10.1016/j.mechmat.2021.104031.

[16] J. Vetrone, J. E. Obregon, E. J. Indacochea, and D. Ozevin. The characterization of deformation stage of metals using acoustic emission combined with nonlinear ultrasonics. *Measurement*, **178**, (2021). https://doi.org/10.1016/j.measurement.2021.109407.

[17] TCVN 1651-1:2018. *Steel for the reinforcement of concrete - Part 1*. Vietnamese National Standard, Ministry of Construction.

[18] Dassault Systèmes®. *Abaqus analysis user's guide*, (2023).

[19] M. Kõrgesaar. The effect of low stress triaxialities and deformation paths on ductile fracture simulations of large shell structures. *Marine Structures*, **63**, (2019), pp. 45–64. https://doi.org/10.1016/j.marstruc.2018.08.004.

[20] S. Marth, H.-A. Häggblad, M. Oldenburg, and R. Östlund. Post necking characterisation for sheet metal materials using full field measurement. *Journal of Materials Processing Technology*, **238**, (2016), pp. 315–324. https://doi.org/10.1016/j.jmatprotec.2016.07.036.

[21] S.-J. Park, B. C. Cerik, and J. Choung. Comparative study on ductile fracture prediction of high-tensile strength marine structural steels. *Ships and Offshore Structures*, **15**, (2020), pp. S208–S219. https://doi.org/10.1080/17445302.2020.1743552.

[22] Z. Yao and W. Wang. Full-range strain-hardening behavior of structural steels: Experimental identification and numerical simulation. *Journal of Constructional Steel Research*, **194**, (2022). https://doi.org/10.1016/j.jcsr.2022.107329.